Human Molecular Genetics, 2011, Vol. 20, No. 18 **3620–3631**
doi:10.1093/hmg/ddr282
Advance Access published on June 16, 2011

Ccdc66 null mutation causes retinal degeneration and dysfunction

Wanda M. Gerding[1,*], Sabrina Schreiber[1], Tobias Schulte-Middelmann[1], Andreia de Castro Marques[3], Jenny Atorf[4], Denis A. Akkad[1], Gabriele Dekomien[1], Jan Kremers[4], Rolf Dermietzel[2], Andreas Gal[5], Thomas Rülicke[6], Saleh Ibrahim[3], Jörg T. Epplen[1,*] and Elisabeth Petrasch-Parwez[2]

[1]Department of Human Genetics and [2]Department of Neuroanatomy and Molecular Brain Research, Ruhr-University, 44780 Bochum, Germany, [3]Department of Dermatology, University Lübeck, 23538 Lübeck, Germany, [4]Department of Ophthalmology, University Hospital Erlangen, 91054 Erlangen, Germany, [5]Department of Human Genetics, University Hospital Hamburg-Eppendorf, 20246 Hamburg, Germany and [6]Institute of Laboratory Animal Science and Biomodels Austria, University of Veterinary Medicine, 1210 Vienna, Austria

Received April 29, 2011; Revised and Accepted June 10, 2011

Retinitis pigmentosa (RP) is a group of human retinal disorders, with more than 100 genes involved in retinal degeneration. Canine and murine models are useful for investigating human RP based on known, naturally occurring mutations. In Schapendoes dogs, for example, a mutation in the *CCDC66* gene has been shown to cause autosomal recessively inherited, generalized progressive retinal atrophy (gPRA), the canine counterpart to RP. Here, a novel mouse model with a disrupted *Ccdc66* gene was investigated to reveal the function of protein CCDC66 and the pathogenesis of this form of gPRA. Homozygous *Ccdc66* mutant mice lack retinal *Ccdc66* RNA and protein expression. Light and electron microscopy reveal an initial degeneration of photoreceptors already at 13 days of age, followed by a slow, progressive retinal degeneration over months. Retinal dysfunction causes reduced scotopic a-wave amplitudes, declining from 1 to 7 months of age as well as an early reduction of the photopic b-wave at 1 month, improving slightly at 7 months, as evidenced by electroretinography. In the retina of the wild-type (WT) mouse, protein CCDC66 is present at highest levels after birth, followed by a decline until adulthood, suggesting a crucial role in early development. Protein CCDC66 is expressed predominantly in the developing rod outer segments as confirmed by subcellular analyses. These findings illustrate that the lack of protein CCDC66 causes early, slow progressive rod–cone dysplasia in the novel *Ccdc66* mutant mouse model, thus providing a sound foundation for the development of therapeutic strategies.

INTRODUCTION

Retinitis pigmentosa (RP) is a genetically heterogeneous group of retinal diseases, with an incidence of approximately 1:3500 (1). Although RP can result from mutations in many different genes, the various forms of disease share phenotypic similarities. Clinically, patients present with an initial loss of night and peripheral vision, followed by a slow, progressive loss of central vision, ultimately leading to blindness (1,2). Currently, no effective treatment is available for the different RP forms (3). Generalized progressive retinal atrophy (gPRA) represents the canine counterpart of RP. Interestingly, in Schapendoes dogs, a mutation in the newly described coiled-coil domain-containing 66 gene (*CCDC66*) has been linked to gPRA and is inherited in an autosomal recessive manner (4). Another mutation in the same gene resulted in gPRA in a

*To whom correspondence should be addressed at: Department of Human Genetics, MA 5/39, Ruhr University Bochum, Universitätsstrasse 150, 44801 Bochum, Germany. Tel: +49 2343223831; Fax: +49 2343214196; Email: wanda.gerding@rub.de (W.M.G.); Department of Human Genetics, MA 5/142, Ruhr University Bochum, Universitätsstrasse 150, 44801 Bochum, Germany. Tel: +49 2343223839; Fax: +49 2343214196; Email: joerg.t.epplen@rub.de (J.T.E.)

mongrel sired by dogs related in first-degree (5). The *CCDC66* gene is evolutionarily conserved in vertebrate species, with a complex pattern of differential RNA splicing, resulting in various isoforms (see UCSC genome browser) (6). In humans, four CCDC66 protein isoforms listed (UniProtKB/Swiss-Prot database, accession no. A2RUB6) are encoded by two 'long' spliced variants (LSV; ~109, ~105 kDa) and one 'short' spliced variant (SSV; ~21 kDa) as well as an experimentally yet unconfirmed ~32 kDa SSV. In the mouse, database information (UniProtKB/Swiss-Prot accession no. QSNS45) comprises an LSV of ~107 kDa, two experimentally unconfirmed LSVs (~103, 90 kDa), whereas SSV appear to be lacking. Protein CCDC66 has been detected in the photoreceptors of mice, dogs and humans, suggesting an important role in the visual cascade of mammals (4). However, genomic investigations of RP families have not yet provided evidence for a linkage of an RP form to a corresponding chromosomal region (A.G., unpublished data). Animal models are very useful for assessing underlying pathophysiological mechanisms and also for working towards novel therapeutic approaches. In order to elucidate functional aspects of protein CCDC66, a mouse with a constitutive *Ccdc66* null mutation was established, and its retinal phenotype characterized. Moreover, the expression of protein CCDC66 was investigated during post-natal murine development, and its subcellular localization in mouse photoreceptors analysed. The consequences of a lack of protein CCDC66 are discussed in relation to an apparently new pathway leading to retinal degeneration, emphasising the key role of CCDC66 in proper retinal function and vision.

RESULTS

Generation of *Ccdc66* null mutation

A null mutation in the *Ccdc66* gene was generated by introducing a gene trap 5′ of murine exon 4 (accession no. NM_177111); the latter includes three possible translation start codons (Fig. 1A). A high proportion (see Supplementary Material, Table S1) of the *CCDC66* splice variants in humans include a homologue of exon 4 in the mouse, as revealed by analysis of human retinal cDNA. The homologous region of the gPRA mutation in the Schapendoes breed of dog is located in exon 5 in the mouse (Fig. 1A). Therefore, the insertion of the gene-trap vector 5′ of exon 4 should result in a disruption of the *Ccdc66* gene without critical protein expression. Following the generation of trapped embryonic stem (ES) cell lines, mutant animals from one of these clones were generated and designated as 129P2;B6N-*Ccdc66*$^{Gt(bgeo)}$. The litters of heterozygous mutants comprised homozygous (−/−), heterozygous (+/−) and WT (+/+) offspring as expected in a Mendelian ratio of 1:2:1. Homozygous −/− mutant mice ascertained by PCR genotyping (Fig. 1B) were viable.

Two results confirmed that the *Ccdc66* gene was inactivated in mutant mice. Quantitative RT–PCR for mouse exons 4–5 revealed no *Ccdc66* transcripts in the retinae of −/− mutants ($P < 0.001$) when compared with reduced levels in +/− ($P < 0.01$) and normal *Ccdc66* expression in WT mice (Fig. 1C). In addition, transcripts of the rod photoreceptor marker *Pde6b* were less abundant in *Ccdc66* −/− mice ($P < 0.001$), intermediately reduced in +/− mice ($P < 0.01$) when compared with WT mice (Fig. 1C), thus indicating a degradation of rod photoreceptors, whereas no significant change in expression of the cone photoreceptor marker *Gnat2* was detected between genotypes, indicating that cones are not primarily involved in retinal degeneration. In 3-month-old mice, western blot analyses of whole-retinal lysates using the commercially available, but yet uncharacterized, T-20 antibody against protein CCDC66 did not detect signals at ~100–140 kDa (expected band size ~107 kDa; LSV) in retinae of *Ccdc66* −/− mutants, whereas a weak high molecular weight band (~100 kDa) was evident. The signal intensities for protein PDE6B paralleled transcription in the retinae (Fig. 1D). The specificity of the T-20 antibody for CCDC66 detection has been verified using excess blocking peptide with the antibody. T-20 antibody binding to the CCDC66 specific epitope was not demonstrable in retinal cell lysates of mouse or human with a weak unspecific ~100 kDa band that also was detectable in *Ccdc66* −/− mice (Fig. 1D). Simultaneously, a strong non-specific band of ~34 kDa appeared in western blot analyses, a signal that was also detectable in *Ccdc66* −/− mice. This non-specific signal might obscure CCDC66-specific immunostaining in the retina. Therefore, the T-20 antibody was not used for immunohistochemistry.

The G-14 antibody against CCDC66 protein showed prominent staining of photoreceptor outer segments in WT retinae of mice (at 1 month of age) lacking in *Ccdc66* −/− littermates, as shown by peroxidase and fluorescence immunohistochemistry (Fig. 1E). Faint staining in the inner retina was observed in both WT and *Ccdc66* −/− mice, and was thus likely to represent unspecific detection. Fluorescence staining with the cone marker Peanut agglutinin (PNA) and CCDC66 revealed no specific co-localization (Fig. 1E), indicating that CCDC66 was not localized in cone but in rod photoreceptors. Co-staining of PNA and PDE6B antibody, which selectively stains rod outer segments, was much fainter in *Ccdc66* −/− retinae when compared with the WT mouse (Fig. 1E), indicating affected rods already at 1 month of age. This finding is in agreement with the reduced *Pde6b* RNA (Fig. 1C) and lower PDE6B protein levels (Fig. 1D), as shown for the *Ccdc66* −/− mouse. In contrast, obvious differences in cone-staining were not observed between *Ccdc66* −/− and WT retinae in mice of corresponding ages (Fig. 1E).

Retinal degeneration in the *Ccdc66* −/− retina

In order to characterize the degeneration, retinae (P1, P4, P8, P10, P13, P15, P19, P24, 1m, 3m, 5m and 7m) were analysed in mouse littermates using semi- and ultra section series. WT (Fig. 2A, E, I, M and Q) and *Ccdc66* +/− mice (Fig. 2B, F, J, N and R) showed normal retinal layers at all ages investigated, *Ccdc66* −/− mice presented initial formation of normal retina up to P10 (data not shown). Malformation of photoreceptors with partly distorted outer and inner segments started to develop around P13 (Fig. 2C and D) prior to their terminal differentiation. The degeneration progressed slowly at P15–P24 (data not shown), 1 (Fig. 2G and H) and 3 months (Fig. 2K and L), when the outer nuclear layer was reduced

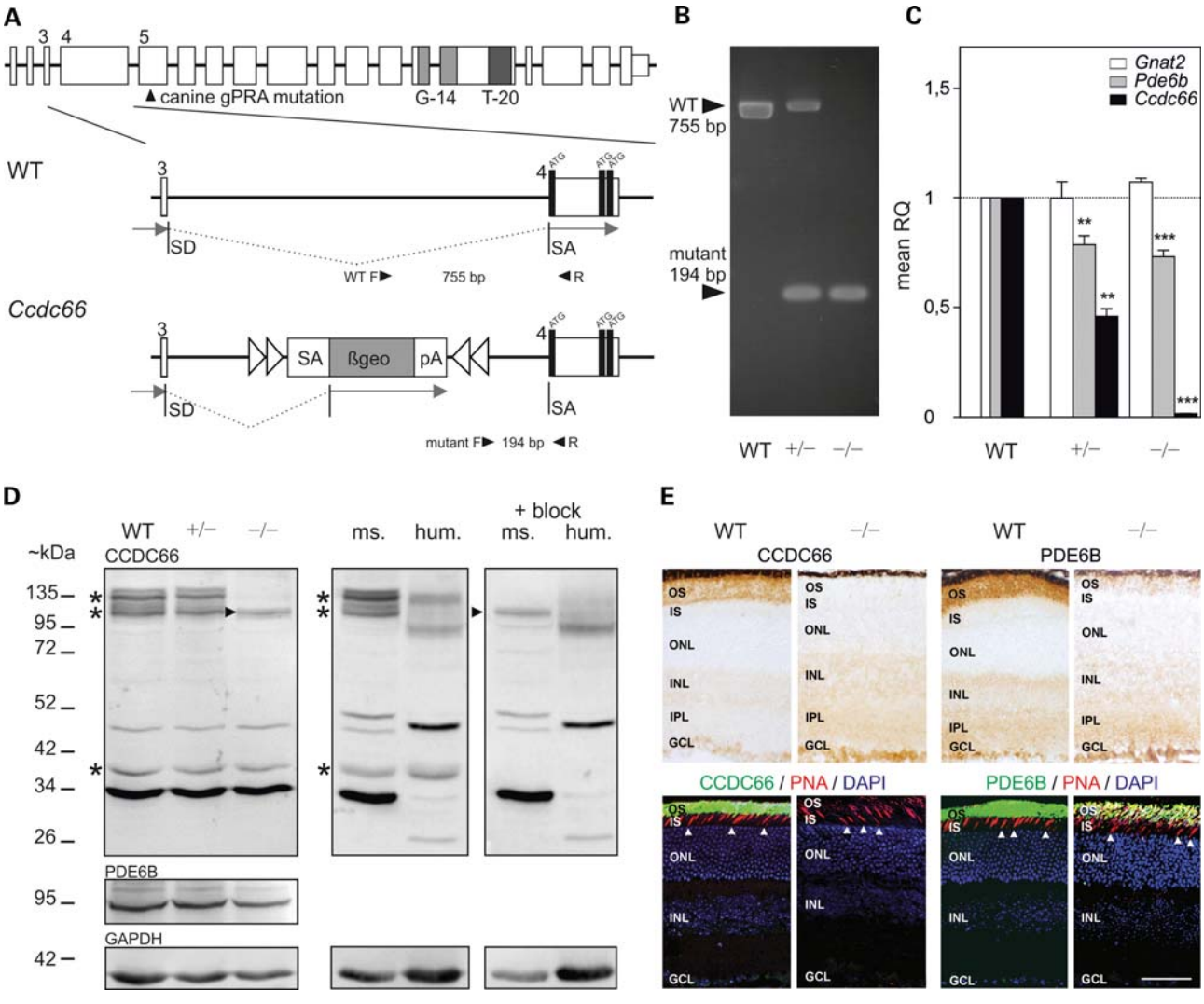

Figure 1. Generation and characterization of the *Ccdc66* gene trap mouse. (**A**) Schematic overview of the mouse *Ccdc66* coding region (top); genomic organization of *Ccdc66* in wild-type (WT) and mutant mice. The homologous region to the canine gPRA mutation in the mouse *Ccdc66* gene is indicated by an arrowhead in mouse exon 5. Genomic sequence regions corresponding to antibody binding regions (G-14 and T-20) in CCDC66 protein are shaded in light and dark grey, respectively. A gene trap is introduced 5′ of exon 4 that can be assessed in WT and gene trap mice using primers indicated by arrowheads. Transcripts (shown as grey arrows) initiated at the endogenous promoter are spliced from the splice donor (SD) of endogenous exon 3 to the splice acceptor (SA) of the SAβgeopA cassette. Thereby the βgeo reporter gene is expressed and the endogenous transcript is captured and prematurely terminated at the cassette's polyadenylation site (pA); SD, splice donor; βgeo, β-galactosidase/neomycin phosphotransferase fusion gene; pA, bovine growth hormone polyadenylation sequence. (**B**) Genotyping by PCR. The 775 bp fragment corresponds to the WT gene, the 194 bp *Ccdc66* mutant fragment is generated from the trapped gene. Results from WT +/+, heterozygous +/− and homozygous −/− mutant mice are shown. (**C**) Quantitative real-time RT–PCR demonstrates the absence of the *Ccdc66* product (exons 4–5) compared with the photoreceptor markers *Gnat2* (cones) and *Pde6b* (rods) in retinal RNA from homozygous −/− mutants in contrast to WT +/+ and heterozygous +/− mice at 3 months of age. Bars indicate the mean relative quantitation (RQ) values (fold change) ± standard deviation of three independent experiments. RQ is compared with WT +/+ expression levels set to 1 (dotted line); RQ values were calculated by the CT method and normalized to *Gapdh* expression. Retinae from $n = 3$ individuals were analysed per genotype. WT +/+ ΔCT values of +/− and −/− mice were compared using a *t*-test ($^{***}P < 0.001$; $^{**}P < 0.01$). (**D**) Western blot analyses using retinal homogenates from 3-month-old WT +/+, heterozygous +/− and *Ccdc66* −/− mice (left). The high molecular weight CCDC66 protein signals at ∼100–140 kDa (expected at ∼107 kDa in the mouse after UniProtKB/Swiss-Prot database) was lacking in homozygous *Ccdc66* −/− mutants (as demonstrated by T-20 antibody) in contrast to the rod photoreceptor marker PDE6B. A low molecular weight CCDC66 signal of ∼37 kDa was detected in mouse and man, possibly indicating an additional retinal CCDC66 isoform. Retinal homogenates from adult C57BL/6J mice (ms.) and human (hum.; center lanes each) were probed with the CCDC66 antibody T-20 or the same antibody pre-incubated with blocking peptide (right lanes each). Arrowheads indicate an unspecific signal at ∼100 kDa detectable in homozygous mutants and WT after excess blocking peptide application. Asterisks denote specific antibody signals prevented by incubation with excess blocking peptide. GAPDH signals represent loading controls. (**E**) CCDC66-peroxidase immunohistochemistry and confocal triple-fluorescence with the cone marker peanut agglutinin (PNA), rod-photoreceptor marker PDE6B and DAPI nuclear counterstaining reveals specific CCDC66 reactivity in outer segments. *Ccdc66* −/− retinae show fainter PDE6B signals. PNA-stained cones are marked by arrowheads. (IS) inner segments, (ONL) outer nuclear layer, (INL) inner nuclear layer, (IPL) inner plexiform layer, (GCL) ganglion cell layer. Bar = 50 μm.

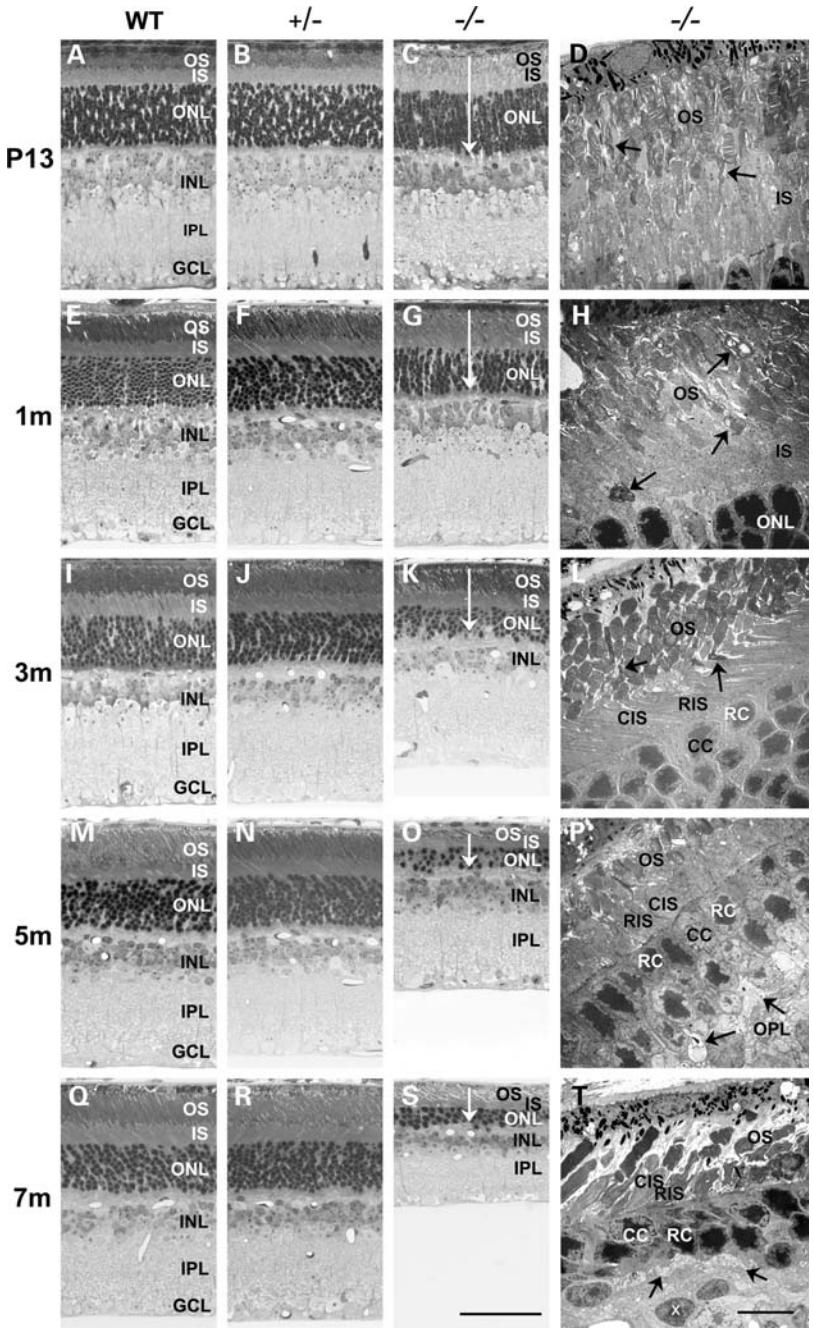

Figure 2. Progressive degeneration of the *Ccdc66* −/− retina. Toluidine-blue stained semi-thin sections showing retinae of wild-type (WT; **A, E, I, M, Q**) and *Ccdc66* +/− mice (**B**, **F**, **J**, **N**, **R**) exhibit normal layers from P13 to 7 months of age (A, B, E, F, I, J, M, N, Q, R) in contrast to the *Ccdc66* −/− retina, which reveals continuous thinning of the outer retina, the thickness of which is marked by white arrows (**C, G, K, O, S**). At P13, the photoreceptors are distorted in the outer (OS) and inner segments (IS) in the *Ccdc66* −/− retina (C) as confirmed by electron microscopy (**D**, arrows). (G) In the *Ccdc66* −/− retina the outer nuclear layer (ONL) is slightly reduced at 1 month. (**H**) Electron microscopy reveals severely distorted and partly condensed IS and OS and debris (arrows). (K) At 3 months, the ONL comprises only 5–6 rows of photoreceptor nuclei. (**L**) In the photoreceptor layer degenerating rod (RIS) and cone inner segments (CIS) as well as cone (CC) and rod cells (RC) are detectable ultrastructurally. (O) At 5 months, the ONL is limited to 2–3 rows, the photoreceptor layer degenerated to a small stripe. (**P**) Electron microscopy exhibits irregularly condensed chromatin in RC and CC; OS and IS are short and thickened. The outer plexiform layer (OPL) shows degenerated pedicles (arrows). (S) At 7 months, the inner retina with the inner nuclear (INL) and inner plexiform layer (IPL) is thinned. (**T**). In the ONL, fragmented nuclei are obvious as well as displaced cells (x) and shrunken pedicles in the OPL (arrows). GCL, ganglion cell layer. Bar in S = 50 μm for A, B, C, E, F, G, I, J, K, M, N, O, Q, R, S; bar in T = 10 μm for D, H, L, P, T.

to 5–6 rows. In the photoreceptor layer, debris and outer segments with disoriented discs were observed (Fig. 2H and L). From 5 to 7 months, only a thin outer nuclear and photoreceptor layer with severely shrunken outer and inner segments was preserved in *Ccdc66* −/− mice (Fig. 2O and S). Remnants represent degenerating rods and cones as

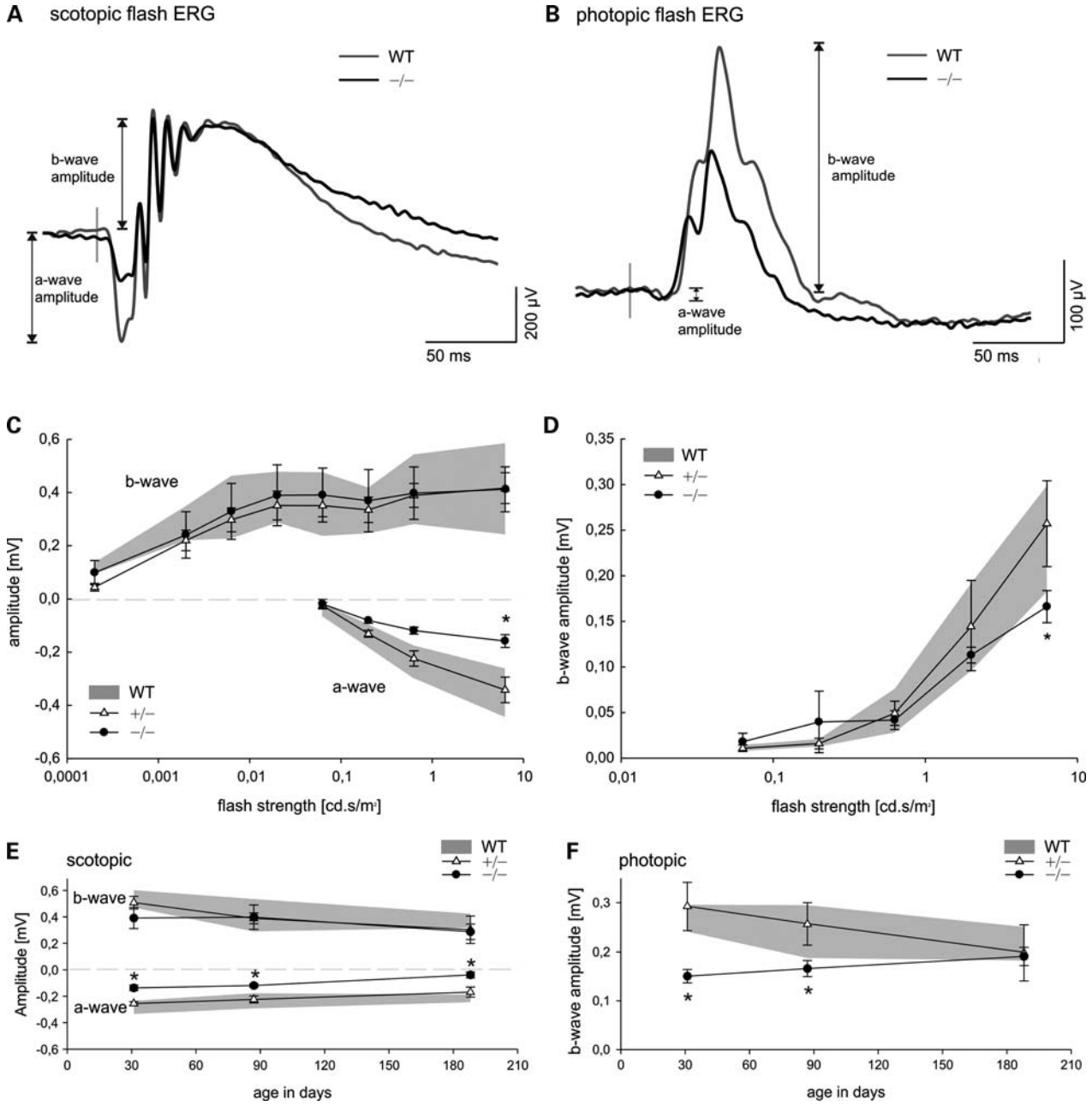

Figure 3. ERG recordings. Effect of CCDC66 deficiency on mouse retinal function in mice under scotopic (**A**, **C**, **E**) and photopic (**B**, **D**, **F**) conditions and age-dependent retinal function at about 1, 2.5–3 (binned) and 7 months of age (E, F). Superimposed ERG recordings from the left eye of a wild-type (WT) and a *Ccdc66* −/− mouse at 3 months reveals a reduced a-wave amplitude under scotopic conditions (A) and a reduced b-wave amplitude under photopic conditions on a background intensity of 25 cd/m^2. (B) Vertical lines in (A) and (B) indicate stimulus onset. Statistical evaluation of ERG a- and b-wave amplitudes for WT +/+, heterozygous +/− and homozygous *Ccdc66* −/− mice at 2.5–3 months of age with mean values and standard deviations as indicated by error bars. Significant differences between *Ccdc66* −/− and WT mice are marked by asterisk (Student's *t*-test, WT versus −/− $P < 0.01$). Mean scotopic (E, at 2.0 cd.s/m^2) and photopic (F, at 6.3 cd.s/m^2) at 1, 2.5–3 and 7 months of age reveals reduced scotopic a-wave amplitude at all ages in *Ccdc66* −/− retinae and an improvement in photopic b-wave amplitude over time in *Ccdc66* −/− mice (significant differences between WT, +/− and *Ccdc66* −/− are marked by asterisk, one-way ANOVA $P < 0.001$).

confirmed ultrastructurally, and the outer plexiform layer contained degenerating pedicles and displaced cells (Fig. 2P and T). Progressive thinning of inner retinal layers suggested secondary affection post-synaptic to degenerated photoreceptors (Fig. 2O and S).

Retinal physiology in *Ccdc66* −/− mice

In order to investigate retinal impairment in *Ccdc66* −/− mice, electroretinography (ERG) was performed in homozygous, heterozygous and WT littermates. Figure 3 displays representative

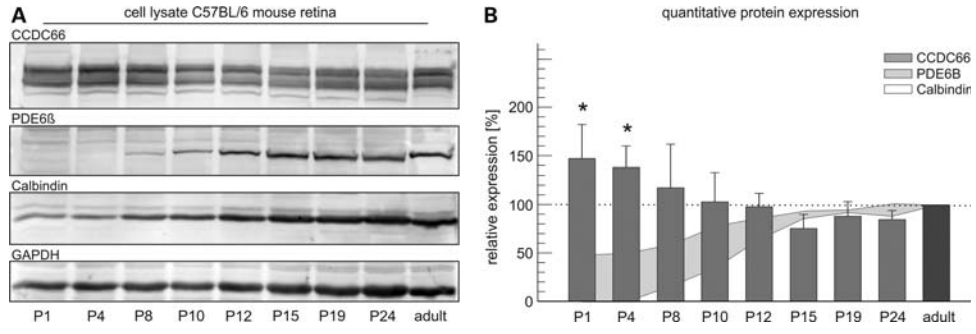

Figure 4. Quantitative CCDC66 protein expression in the murine retina. (**A**) Developmental protein expression levels of CCDC66, Calbindin and PDE6B in retinal cell lysates of C57BL/6J mice were analysed by western blot analysis (G-20 antibody), GAPDH protein was probed as loading control. Forty microgram protein/lane was applied on a 10% SDS gel. (**B**) Quantitative expression of CCDC66, PDE6B and calbindin in retinae of C57BL/6J mice were normalized to GAPDH, and adult expression level was set to 100%. Significantly higher expression levels of CCDC66 are evident at P1 and P4 when compared with adult age (*t*-test, $^*P < 0.05$). $n = 3$ retinae were analysed per developmental stage in three independent experiments.

scotopic (mainly rod-driven) and photopic (cone-driven) flash ERG responses in these mice. In parallel with morphological degeneration, ERG measurements showed signs of incipiently impaired photoreceptor function in *Ccdc66* −/− mice at 2.5 or 3 months of age. The mean scotopic a-wave amplitude, a measure of photoreceptor integrity, was reduced up to 54% in mice harboring the null mutation in homozygous state ($P < 0.01$; Fig. 3C). Photopic cone ERGs showed that b-wave amplitude was reduced up to 70% ($P < 0.01$; Fig. 3D), indicating slightly impaired function at a post-photoreceptoral level. Early functional visual impairment of the *Ccdc66* −/− retina was already detectable at 1 month of age, progressing slightly until 7 months of age, as demonstrated by a reduced scotopic a-wave amplitude, reflecting rod-photoreceptor degradation (Fig. 3E). Interestingly, the photopic b-wave amplitude revealed intense impairment already at 1 month of age, but it improved again until 7 months, almost reaching WT levels (Fig. 3F). This finding/information indicates that cone-driven post-photoreceptoral impairment is highest at an early age and might be compensated for over time. There were no differences in a- and b-wave latencies between WT, *Ccdc66* +/− and −/− mice at all ages investigated.

Post-natal protein expression and spatiotemporal localization of protein CCDC66 in mouse retinal development

In order to elucidate functional aspects of protein CCDC66 for the visual cascade, the developmental time course of retinal CCDC66 (T-20 antibody) expression was characterized by quantitative western blot analyses at post-natal stages from P1 into adulthood (Fig. 4A and B). CCDC66, like Calbindin, was detected at all points in time, in contrast to the retinal rod-photoreceptor marker PDE6B (Fig. 4A). Highest retinal CCDC66 levels were observed at P1 and P4, declining thereafter, with steady levels from P12 to adulthood. This time course contrasted that of PDE6B expression, commencing around P4/P8, parallel to rod specialization (7) and augmenting into adulthood, a similar expression pattern like Calbindin (Fig. 4B). Post-natal CCDC66 expression was also investigated by double fluorescence immunostaining (CCDC66 stained by G-14 antibody either with PNA or Rhodopsin) and Toluidine blue-stained semi-thin sections as morphological reference (Fig. 5). In the WT retina, CCDC66 was detectable earliest at P8 in the growing photoreceptors (Fig. 5B), whereas at P1 and P4 no CCDC66 signal was evident. CCDC66 immunoreactivity increased in the outer segments from P12 to P19 (Fig. 5G, L and Q) paralleling the differentiation of outer segments (Fig. 5F, K and P). No specific co-localization with CCDC66 was identified in PNA-stained, growing cones, suggesting that CCDC66 may selectively label rod outer segments. Yet, double immunofluorescence with CCDC66 and Rhodopsin, specifically staining rod photoreceptors, revealed co-localization of CCDC66 and Rhodopsin at P8, augmenting to P19 (Fig. 5D, I, N and S) in WT retinae; co-localization was restricted to the outer segments. *Ccdc66* −/− retinae lacked CCDC66 expression (Fig. 5C, E, H, J, M, O, R and T). After eye opening around P15, Rhodopsin staining was reduced in the outer segments of the *Ccdc66* −/− retina similar to PDE6B staining (Fig. 1E). Pre-embedding peroxidase-immunostained semi-thin section of P15 WT retinae (Fig. 5U) as well as silver-enhanced immunogold post-embedding electron microscopy confirmed CCDC66 in the outer segments (Fig. 5V and W).

CCDC66 mutations in human retinal disease

The presence of CCDC66 protein was confirmed in the photoreceptors of healthy mouse and human retinae (4). In order to address the question as to whether CCDC66 deficiency causes retinal disease also in humans, thorough sequence analyses of the *CCDC66* gene have been performed in 80 RP and 20 Leber congenital amaurosis (LCA) patients (see Supplementary Material, Table S2). In total, 28 sequence variations were identified in the 20 exons of the human *CCDC66* gene (NM_001012506), of which seven are not yet published (IVS5−14A>G; c.2042G>A p.Cys681Tyr; IVS18+21_24 Ins TCAA; IVS17−17 del A; 3'UTRc.2702_2706InsCTTC; 3'UTRc.2785T>C). In addition, sequence variation in exon 16, resulting in an amino acid exchange (c.2042G>A p.Cys681Tyr), was detected in an RP patient in heterozygous state, but not in 172 healthy controls. Re-sequencing the entire *CCDC66* gene of this patient revealed no other relevant variation.

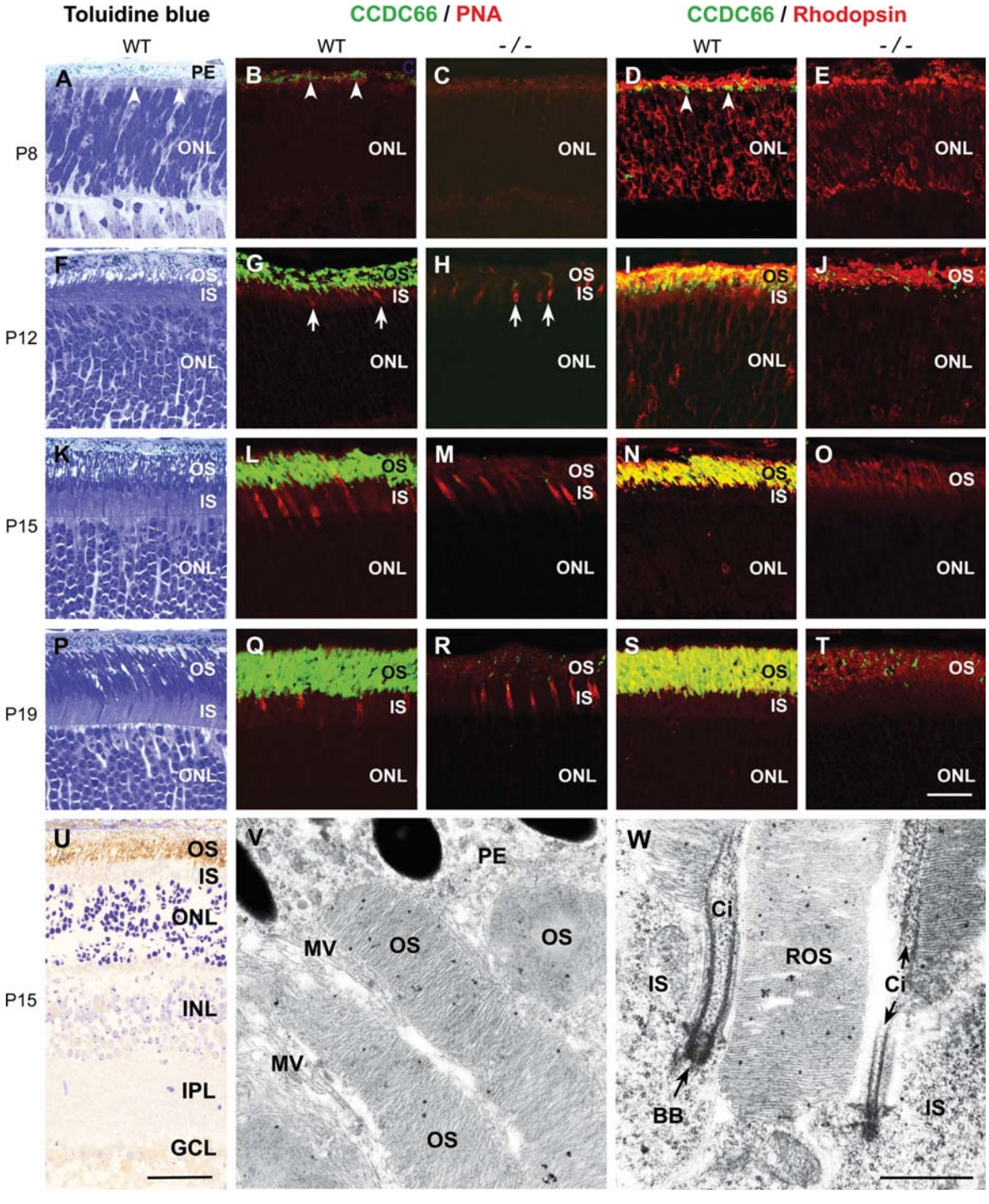

Figure 5. CCDC66 expression in the murine retina as demonstrated by immunohistochemistry. Retinal CCDC66 distribution in merged double fluorescence-immunostaining at stage P8 to P19 in wild-type (WT) and *Ccdc66* −/− mice with corresponding Toluidine blue-stained semi-thin sections as morphological reference (**A**, **F**, **K**, **P**). At P8, CCDC66 (D, green) is faintly expressed in developing photoreceptors (**B** arrowheads), increases progressively in differentiating outer segments (OS) at P12 to P19 (**G**, **L**, **Q**). *Ccdc66* −/− mice lack specific CCDC66 reactivity at the stages investigated (**C**, **H**, **M**, **R**). Co-staining with the cone marker peanut agglutinin (PNA red; G, H, arrows) exhibits no obvious differences between WT and *Ccdc66* −/− retinae. Co-staining of CCDC66 with the rod marker Rhodopsin (red) shows co-localization from P8 to P19 (**D**, arrowheads, **I, N, S**) in WT but not in age-matched Ccdc66 −/− retinae (**E, J, O, T**). (**U**) CCDC66-Peroxidase-immunostained semi-thin section counterstained with Toluidine blue confirms OS localization. (**V**) Silver-enhanced immunogold electron microscopy displays particles distributed in the OS but not in pigment epithelium (PE) and microvilli (MV). (**W**) In the inner segments (IS), connecting cilium (Ci) and basal body (BB) single gold particles occur. ONL, outer nuclear layer; INL, inner nuclear layer; IPL, inner plexiform layer; GCL, ganglion cell layer; ROS, rod outer segment. Bar in T = 20 μm for (A–T); bar in U = 50 μm, bar in W for (V, W) = 1 μm.

DISCUSSION

The genetically modified mouse, which lacks *Ccdc66* expression and has a retinal phenotype, extends earlier studies of *CCDC66* mutations linked to gPRA (4). CCDC66 appears as an essential photoreceptor protein in vertebrates with functional relevance in early murine retinal development. A lack of protein CCDC66 in the novel *Ccdc66* −/− mouse leads to an early photoreceptor degeneration, with a slow, progressive retinal phenotype and physiological impairment of the retina.

Retinal degeneration in *Ccdc66* −/− mice

Like in *Ccdc66* −/− mice, gPRA dogs exhibit early, progressive retinal degeneration with both rods and cones being affected. The disease onset in Schapendoes dogs, with a mean life span of 12–15 years, ranges between 4 and 7 years of age (4). Yet, retinal degeneration in Schapendoes dogs is not as well documented. In *Ccdc66* −/− mice, retinal degeneration is morphologically evident at 13 days of age, with initial severe affection of rod and cone photoreceptors, followed by a slow, progressive degeneration of the outer and, at advanced age, also of the inner retina. Both progressive degeneration and functional impairment, as measured by ERG, can be detected from 1 to 7 months of age. When relating retinal degeneration and mean life expectancy (∼2 years), disease onset appears comparatively earlier in mice. Yet, retinal degeneration in dogs might be less evident clinically. Compared with other models of gPRA and retinal degeneration in the mouse, the present study paves the way for early, decisive phenotyping and progression studies. Hence, it allows an evaluation of new pathways in which CCDC66 is crucially involved.

As reported earlier, *Ccdc66* RNA appears to be spliced in a complex manner (4). In the *Ccdc66* −/− mouse, LSV is abolished, whereas SSV coding for a CCDC66 isoform of ∼40 kDa is apparently present in the retina, according to the western blot (blocking) results. The existence of LSV and SSV isoforms has already been deduced in humans (UniProt/Swiss-Prot database accession no. A2RUB6). A short isoform has not been reported for the mouse to date. Yet, based on our data, a short isoform is expressed in the mouse retina. This isoform is not sufficient to compensate for the loss of LSV leading to retinal degeneration. Further studies are required to unequivocally elucidate the specific relevance of CCDC66 isoforms in retinal functioning.

CCDC66 expression during post-natal development

High retinal CCDC66 expression, directly after birth and prior to the formation of rods and cones, might be involved in early retinal maturation, possibly even before birth. The strong CCDC66 signal of ∼100–140 kDa corresponding to LSV was already detectable at P1 in western blots following an analysis using T-20 antibody. This finding is in contrast to CCDC66 expression analyses using the G-14 antibody in retinal tissue, where CCDC66 was not detectable before P8. Although it is not entirely clear how this difference in post-natal expression occurs, we suspect that both antibodies detect different retinal CCDC66 protein isoforms. For example, in the western blot experiments using the T-20 antibody, another specific signal of a distinct size (∼ 40 kDa) could be demonstrated. Whether this corresponds to a specific short isoform in the mouse retina needs to be elucidated in further studies. Alternative antibodies are to be employed, because both commercially available antibodies of this study reveal either inconsistent results in western blot (T-20) or immunohistochemistry (G-14). Yet, both antibodies revealed a specific retinal signal which was not present in the *Ccdc66* −/− mouse. Further study of retinal isoforms could also help to characterize the specific role of this novel protein in retinal development. As evidenced by immunohistochemistry, the pronounced CCDC66 expression in outer segments of the photoreceptor parallels development in the outer segment of the rod. Interestingly, the degeneration of the photoreceptor starts around eye-opening, also correlating with a rapidly increasing CCDC66 expression in the outer segments.

Retinal dysfunction in *Ccdc66* mutant mice

The ERG provides an overall electrical response of the eye, comprising different components (8), and the functional integrity of various retinal structures can be assessed accordingly. Information processing mechanisms can be evaluated as well as the sites of retinal disorder (8). ERG data in *Ccdc66* −/− mice reflect advanced degeneration of photoreceptors at the age of 1, 3 and 7 months, which manifests itself as a change in a scotopic (rod-driven) a-wave amplitude. In addition, the reduced photopic b-wave amplitude at 1 and 3 months also implies a deficit at the post-photoreceptor level. At 7 months of age, the photopic b-wave is slightly improved and reaches WT levels. Even if the age-dependent improvement is only very small, it might be substantial, taking into account that the WT and +/− mice display a decrease in photopic b-wave amplitude. This effect may not be important considering that 97% of the photoreceptors are rods and only 3% cones (9). However, even cones remain functional in the absence of an outer segment (10). It is tempting to speculate that, in the *Ccdc66* −/− mouse, some of the remaining cones (whether complete or possibly including a functional inner segment) could compensate, at least to some extent, for the severe rod-photoreceptor degradation. At 3 months of age, RNA expression of the cone marker *Gnat2* is not reduced in the *Ccdc66* −/− retina, and it even appears to be slightly increased (not reaching significance level). This finding suggests sustained functionality of cone photoreceptors in the *Ccdc66* −/− mouse, despite the severely degenerated rods. In conclusion, in accordance with morphological observations, these physiological data suggest that the combined rod–cone retinopathy in the *Ccdc66* −/− mouse is predominantly present in the rod photoreceptors. The ERG measurements show overall an early, slow, progressive impairment of photoreceptor function. Comparing these mouse ERG data to those for humans, severe loss of vision occurs in cone–rod dystrophy earlier than in RP. In cone–rod dystrophy, the ERG a- and b-wave delays are early disease signs, occurring before a- and b-wave amplitude reduction (2). These retinopathy signs in cone–rod dystrophy in humans are in contrast to the *Ccdc66* −/− model of retinal

degeneration in mice, showing no differences in a- and b-wave delay at 3 months of age. Thus, the ERG data do not resemble cone–rod dystrophy in humans, rather RP, in which degeneration is accompanied by a significant reduction in b-wave amplitude without a- or b-wave delay. Moreover, the RP phenotypes occur relatively early, and slow degeneration is evident in the *Ccdc66* mouse model compared with other RP mouse models, such as *rd1* and *rd10*, in which degeneration shows a relatively rapid progression (11). The ERG data for the *Ccdc66* −/− mouse clearly point to primary rod degeneration accompanied, to a lesser extent, by cone degeneration, following a time course comparable with typical RP in humans. Interestingly, photopic b-waves improve over time and, even after 3 months, *Ccdc66* −/− mice might reveal a trend toward an increased RNA expression of the cone marker *Gnat2*, suggesting an increase in cone photoreceptor expression. The role of cone photoreceptors in the *Ccdc66* −/− mouse should be elucidated in future studies. The mouse retina is dominated by rods, but in the periphery cone numbers equals the cone densities in humans (12). Therefore, based on human immunohistochemistry data, it remains to be established how CCDC66 deficiency would manifest itself in humans, particularly in the fovea, where exclusively cones are located, in contrast to the retinal periphery. Hence, any human phenotype cannot be predicted. On the other hand, pronounced retinal phenotypes in mouse and dog indicate general pathogenetic mechanisms resulting from CCDC66 deficiency. Based on the canine and mouse data, CCDC66 dysfunction induces retinal degeneration, following autosomal recessive inheritance. Thus, in the future, patients with unknown cause(s) of retinal degeneration will be investigated. Although a sole mutation in heterozygous state was found in one RP patient, it is unlikely that RP in this patient was due to this mutation. Nevertheless, the number of patients investigated for *CCDC66* mutations is limited in relation to the high number of genes associated with different types of RP and LCA in humans (13,14).

Mouse models for retinal degeneration and the study of RP

In general, many mouse models for RP exhibit rapid retinal dysfunction (11). Hart *et al*. (15) examined genotype–phenotype correlations of mouse *Pde6b* mutations, the underlying cause for autosomal-recessively inherited RP in humans (16) and found mutation-dependent phenotypes of retinal degeneration. The classic $Pde6b^{rd1}$ mouse model was the first RP mouse model, characterized by rapid photoreceptor degeneration 8 days after birth and by a loss of nearly all photoreceptors by 3 weeks of age (11). In contrast, atypical retinal degeneration models ($Pde6b^{atrd1\text{-}3}$) exhibit almost normal retinae at 3 weeks of age, thus resembling a slow degeneration model and sharing the phenotype common for human patients with RP, in which degeneration usually has a slow progression. This progression typifies rod–cone dystrophy, for which degeneration is initiated by the loss of night-vision, followed by loss of day-light vision after several years (2). Therefore, the slow, progressive degeneration described here appears particularly advantageous for retinal investigations, because it reflects a typical course for RP in humans.

In conclusion, the *Ccdc66* mutant mouse introduced here and which is characterized by an early, slow, progressive retinal degeneration provides a useful model for a range of future studies focused on elucidating the spectrum of molecular mechanisms involved in retinal photoreceptor degeneration as in human RP. This mouse model should also provide a valuable tool to explore the precise role of the protein CCDC66 in the context of photoreceptor development and maintenance, thus providing additional insights into the basics of vertebrate photoreceptor organization and function.

MATERIALS AND METHODS

Animals and human tissue

Mice of the C57BL/6J strain were obtained from Jackson Laboratory (Bar Harbor, ME, USA), bred at the Ruhr-University Bochum (RUB) and kept in a light/dark cycle of 12 h/12 h). The mice had unlimited access to commercial food and water. *Ccdc66* gene trap mice were generated and bred as described subsequently. All experimental procedures complied with the regulations of the University of Michigan Committee on Use and Care of Animals (for mice) and the Ministry of Science and Public Health of the City State of Hamburg, Germany (for human DNA). The ERG experiments were performed in accordance with the guidelines for the use of animals of the Association for Research in Vision and Ophthalmology and were approved by the Animal Welfare Authority (Government of von Mittelfranken, Ansbach, Germany).

Loss-of-function mutation of *Ccdc66* and genotyping of mutant mice

A gene trap clone (E021F10) was purchased from the German Gene Trap Consortium (GGTC). The generation and characterization of GGTC gene trap clones has been described previously (17,18). The E021F10 clone was generated using the rFRosabgeo+1s-targeting vector (17), which has a cassette containing a splice acceptor site, a β-galactosidase/neomycin phosphotransferase fusion gene (ßgeo) and a bovine polyadenylation site. ES cells were expanded on a feeder layer of mouse embryo fibroblasts which had been pre-treated with mitomycin C (Sigma). Tissue culture dishes were coated with 0.1% gelatine (Sigma), and the cells were maintained in the medium GMEM (Sigma, G5154) supplemented with 15% ES cell qualified foetal bovine serum (PAN Biotech), non-essential amino acid solution (PAA, Austria), 1 mM sodium pyruvate, 2 mM stable glutamine (PAA), penicillin/streptomycin, 0.1 mM β-mercapto-ethanol (Sigma) and 1000 iU/ml of murine leukemia inhibitory factor (Millipore, Vienna, Austria). For the injection of the morula stage, ES cells were trypsinized with 0.05% trypsin/EDTA (Sigma) for 10 min and re-suspended in ES cell medium to achieve a single cell suspension. For feeder-cell depletion ES cells were re-plated on a fresh tissue culture dish and incubated at 37°C for 45 min. Supernatants were discarded, and the remaining, loosely adhering ES cells were rinsed from the plate using ES medium. After centrifugation at 800*g*, the cell pellet was re-suspended for injection in a small volume of ES medium containing 500 iU/ml of DNAse (Invitrogen). As host

embryos for the ES cells, we used morula stages flushed from the oviducts of super-ovulated BALB/c females. ES cells ($n = 8–10$) were injected under the zona pellucida of each embryo. During overnight culture in M16 medium (Sigma M7292), the embryos developed into blastocysts, which were then transferred into the uterus horns of pseudopregnant surrogate mothers 2.5 days post-coitum. Offspring were examined for chimerism, and chimeric males were mated with C57BL/6N WT females, in order to demonstrate germ-line transmission of the mutated allele. Mutant mice were back-crossed to a C57BL/6J background for one generation and routinely genotyped by PCR using a forward (fwd) primer specific for the WT allele as well as the entrapment vector and a common reverse (rev) primer (5′-3′): WT fwd: 5′-GAGAGCAGGCGAGAGGTTTA-3′; gene trap rev: 5′-GCTAGCTTGCCAAACCTACAGGTGG-3′; common rev: 5′-CAAATTGCAAAATG TCCTTT-3′. The sizes of the PCR products were 755 bp (WT) and 149 bp (gene trap).

Quantitative PCR (qPCR), western blot and mutation analyses

After sublethal anaesthetization with CO_2, mice were decapitated and the eyes were enucleated and hemisected at the ora serrata. Retinae were dissected in phosphate-buffered saline (PBS) and snap-frozen in liquid nitrogen and stored for subsequent RNA and protein analyses. RNA was extracted with PeqGold TriFast reagent (Peqlab, Erlangen, Germany) and purified using the RNeasy kit (Qiagen). For qPCR, 30 ng of RNA were used per reaction with the PowerSYBR green RNA-to-C_T™ kit and StepOne Plus device and software (Applied Biosystems) following the manufacturer's instructions. PCR primers were designed to span an exon boundary to avoid the amplification of genomic DNA. Primer sequences for *Ccdc66* (4), *Pde6b* (19), *Gnat2* (20) and the internal standard *Gapdh* (19) have been reported previously. PCR cycling conditions for reverse transcription one-step PCR were as recommended by the manufacturer (StepOne Software™ v2.1, Applied Biosystems). Relative RNA expression was determined from triplicates of three independent assays by the $2^{-\triangle Ct}$ method (21), statistical analysis was performed using Student's *t*-test.

Western blot analysis was conducted as described previously (4). Briefly, whole retinal proteins from human and mouse tissue were extracted in ice-cold lysis buffer [50 mM Tris–HCl (pH 8,0), 150 mM NaCl, 1% (v/v) NP-40, 1 g/l SDS, 1 g/l Na-Desoxycholate) with protease inhibitor cocktail (Sigma-Aldrich, St Louis, MO, USA) on ice for 20 min, centrifuged at 600*g* for 20 min, and then supernatants were harvested and stored at −20°C. Protein quantification was performed according to a standard method (22). After denaturation at 40°C, proteins (40 μg) were loaded on 10% SDS–PAGE and transferred onto nitrocellulose (Hybond C, GE Healthcare) and incubated with polyclonal rabbit anti-CCDC66 antibody (T-20, Santa Cruz Biotechnology Inc.) at a dilution of 1:200. In addition, the specificity of the T-20 antibody was tested by incubating the antibody with the immunizing peptide (20-fold excess, T-20P, Santa Cruz Biotechnology Inc.) prior to membrane incubation. Using HRP-coupled goat anti-rabbit antibody (1:5000 dilution; Jackson ImmunoResearch, USA) as a conjugate, detection was carried out using ECL plus (GE Healthcare) and scanner (Storm 860, GE Healthcare). Blots were stripped (4) and re-probed with polyclonal rabbit anti-PDE6B (1:1000 dilution; Thermo Scientific, Waltham, MA, USA), Calbindin D-28k (1:10000; CB38, Bellinzona, Switzerland) and rabbit anti-GAPDH (1:500 dilution, ab9485, Abcam, UK) as a loading control. The relative protein expression was quantified using the imageJ 1.35i analysis tool (Wayne Rasband, National Institutes of Health, USA) by measuring the integrated optical density of bands and subsequent normalization to GAPDH expression.

Mutation screening in 80 RP and 20 LCA patients was performed in all 20 exons of the *CCDC66* gene, including the flanking intronic areas, using PCR-based single-strand conformation polymorphism (SSCP) analysis (23). Amplicons representing conspicuous banding patterns were sequenced (MegaBace 1000, GE Healthcare, Freiburg, Germany) to detect the underlying nucleotide variations. All patients had typical subjective symptoms and psychophysical signs of a bilateral progressive retinal dystrophy, and were diagnosed by RP/congenital amaurosis of type Leber following a standard ophthalmological examination. DNA samples of the patients studied here were screened previously (by PCR, SSCP and direct sequencing) for mutations in a number of genes for autosomal recessive RP and congenital amaurosis of type Leber, such as *RHO*, *TULP1*, *PDEA*, *PDEB*, *SAG*, *RPE65*, *RDH12*, *MERTK*, *LRAT* and *RP28* but did not carry a disease-relevant sequence variant in any of these genes. Based on family history, retinal dystrophy was inferred to be transmitted autosomal recessively in ∼20% of the cases, whereas the majority of other patients represented sporadic cases with no suspicion for an X-linked pattern of inheritance. Nevertheless, our previous experience suggests that many sporadic cases suffer from autosomal-recessively inherited disease.

Conventional electron microscopy

Mice ($n = 3$ of each genotype and age) were deeply anaesthetized by intraperitoneal injection with pentobarbital (720 mg/kg Nembutal, Merial GmbH, Hallbergmoos, Germany) and perfused transcardially with 2% glutaraldehyde in 0.1 M cacodylate buffer (pH 7.4) for 20 min. The eyes were enucleated and fixed overnight in the same solution. Younger mice (P1–P19) were anaesthetized by asphyxiation in CO_2, decapitated and the eyes enucleated and fixed by immersion for 2 days. All eyes were rinsed in 0.1 M cacodylate buffer and immersed in 4% osmium tetroxide for 3 h, washed and embedded in Araldite (24). Embedded eyes were cut sagittally at the level of the optic nerve and prepared for semi-thin serial sectioning. Ultra-thin sections were contrasted and documented (24).

Light and electron microscopic immunohistochemistry

Mice were anaesthetized and trans-cardially perfused or immersion-fixed with 4% paraformaldehyde (PFA) in 0.1 M sodium phosphate buffer (pH 7.4). Enucleated eyes were rinsed in PBS, immersed overnight in 30% saccharose in

PBS, then shock-frozen and immunostained (24). Light microscopic immunohistochemistry was performed on 12 μm cryosections mounted on Superfrost Plus slides (Menzel, Braunschweig, Germany) and heat dried for 2 h at 40°C. Sections were peroxidase- (25) or fluorescence-immunostained (24). For CCDC66 staining, G-14 antibody (sc-102418; Santa Cruz Biotechnology Inc., 1:20 for fluorescence, 1:100 for peroxidase and immunogold) was applied. Monoclonal a-Rhodopsin antibody (MAB5316, Chemicon, USA; 1:3000 dilution) and polyclonal PDE6B-antibody (Pa1–722, Thermo Scientific, USA; 1:1000) were used for rod photoreceptor staining. Fluorescin isothiocyanate-conjugated PNA-lectin (Molecular Probes; 1:1000 dilution) was used to detect cone photoreceptors. Overview fluorescence sections (Fig. 1E) were cover-slipped with ProLong® Gold antifade reagent with DAPI (Molecular Probes) for nuclear staining. Mouse sections for pre-embedding electron microscopic immunohistochemistry were cut into 50 μm cryosections, immunostained without Triton, fixed with 1% osmium tetroxide and then flat-embedded in Araldite (25). For post-embedding immunogold-labelling, 50 μm retinal vibratome sections were post-fixed with 2% osmium tetroxide for 1 h and flat-embedded in Araldite. For immunogold labelling (26), incubation with the primary CCDC66 antibody was followed by treatment with gold-labelled goat anti-rabbit immunoglobulin (10 nm, Aurion, The Netherlands). The reaction was enhanced (silver kit, Aurion) and finally contrasted with uranyl acetate and lead citrate (24).

ERG recordings

Ganzfeld ERGs were recorded for both eyes of four homozygous *Ccdc66* −/− mice as well as for three heterozygous +/− and four WT littermates (aged 2.5–3 months) and data binned into 87 days for analysis; three WT, two heterozygous +/− and four homozygous −/− mice at 1 month and two WT, two heterozygous +/− and two −/− at 7 months (188 days) of age. The procedure has been described previously (27). Briefly, mice were dark-adapted overnight. Initial preparation was performed under deep red illumination. The animals were anaesthetized by an intramuscular injection of ketamine (50 mg/kg) and xylazine (10.5 mg/kg), and pupils were dilated with a drop of tropicamide (Mydriaticum Stulln®, 5.0 mg/ml, Pharma) and phenylephrine hydrochloride (Neosynephrin POS® 5%, Ursapharm). Contact lens electrodes for mice (Mayo Corporation, Japan) were covered with physiological saline and placed on the corneal surface. Reference and ground electrodes were placed subcutaneously medially to the ears and in the tail, respectively. All stimuli were presented in a Ganzfeld bowl (Roland Consult Q450 SC). At first, the ERG responses to scotopic stimuli were recorded. These stimuli consisted of short flashes of increasing strength, ranging from 0.0002 to 6.3 log cd.s/m^2. At each flash strength, 6–12 responses were averaged. After recording the scotopic ERGs, the eyes were light adapted to a background of 25 cd/m^2. Subsequently, photopic ERG responses were elicited by presenting flashes of increasing strength (0.063, 0.2, 0.63, 2.0 and 6.3 cd.s/m^2) in addition to the background light. Further analysis of the responses was performed offline using self-written routines in Matlab® (©1994–2010 The Mathworks, Inc.). The amplitude of the scotopic a-wave was measured as the difference between the baseline before the onset of the stimulus (30 ms pre-trigger time) and the minimum of the a-wave trough. The scotopic b-wave amplitude was defined as the difference between baseline and b-wave maximum. The b-wave amplitude is commonly measured as the difference between the a-wave trough and the b-wave maximum, in which a- and b-wave amplitudes can be confounded. The more conservative way of measuring the b-wave amplitude was preferred, in order to exclude the possibility that a change in the a-wave amplitude is also reflected in a change of the b-wave amplitude. Of the photopic ERG responses, only the b-wave amplitude was considered for analysis because of the low photopic a-wave amplitude in the mouse (28). Statistical analysis of differences between WT controls and *Ccdc66* −/− mice at 3 months of age was performed using the Student's *t*-test. Differences between the groups age and genotype of ERG a- and b-wave amplitudes for photopic (2.0 cd.s/m^2) and scotopic stimuli (6.3 cd.s/m^2) were tested as one-way or two-way analysis of variance (ANOVA). When two-way ANOVA showed significant interaction, one-way ANOVA tests were performed for each age and genotype. A *P*-value of < 0.01 was considered significant for all statistical measurements. Two days after the ERG measurements, the animals were exposed a sub-lethal dose of CO_2 and then decapitated. Eyes were enucleated for biochemical or histological examination of the retinae.

SUPPLEMENTARY MATERIAL

Supplementary Material is available at *HMG* online.

ACKNOWLEDGEMENTS

The excellent technical assistance of Marlen Löbbecke-Schumacher, Hans-Werner Habbes, Michaela Hagedorn, Meike Kallenbach and Lill Andersen is gratefully acknowledged. The gene trap clone was obtained from the German Gene Trap Consortium.

Conflict of Interest statement. None declared.

FUNDING

This study was supported by German Research Foundation Grant DFG (EP 7/17–1) to J.T.E. and the Austrian Federal Ministry of Science and Research GENAU grant 'Austromouse' to T.R.

REFERENCES

1. Berger, W., Kloeckener-Gruissem, B. and Neidhardt, J. (2010) The molecular basis of human retinal and vitreoretinal diseases. *Prog. Retin. Eye Res.*, **29**, 335–375.
2. Hamel, C. (2006) Retinitis pigmentosa. *Orphanet J. Rare Dis.*, **1**, 40.
3. Shintani, K., Shechtman, O.D. and Gurwood, A.S. (2009) Review and update: current treatment trends for patients with retinitis pigmentosa. *Optometry*, **80**, 384–401.
4. Dekomien, G., Vollrath, C., Petrasch-Parwez, E., Boevé, M.H., Akkad, D.A., Gerding, W.M. and Epplen, J.T. (2010) Progressive retinal atrophy

in Schapendoes dogs: mutation of the newly identified *CCDC66* gene. *Neurogenetics*, **11**, 163–174.
5. Schulte-Middelmann, T. (2009) CCDC66 bei Mensch und Hund. Diploma thesis, Faculty for Biology and Biotechnology, Ruhr University, Germany.
6. Kent, W.J., Sugnet, C.W., Furey, T.S., Roskin, K.M., Pringle, T.H., Zahler, A.M. and Haussler, D. (2002) The human genome browser at UCSC. *Genome Res.*, **12**, 996–1006.
7. Olney, J.W. (1968) An electron microscopic study of synapse formation, receptor outer segment development, and other aspects of developing mouse retina. *Invest. Ophthalmol.*, **7**, 250–268.
8. Hartong, D.T., Berson, E.L. and Dryja, T.P. (2006) Retinitis pigmentosa. *Lancet*, **368**, 1795–1809.
9. Carter-Dawson, L.D. and LaVail, M.M. (1979) Rods and cones in the mouse retina. I. Structural analysis using light and electron microscopy. *J. Comp. Neurol.*, **15**, 245–262.
10. Daniele, L.L., Insinna, C., Chance, R., Wang, J., Nikonov, S.S. and Pugh, E.N. Jr (2011) A mouse M-opsin monochromat: retinal cone photoreceptors have increased M-opsin expression when S-opsin is knocked out. *Vision Res.*, **23**, 447–58.
11. Baehr, W. and Frederick, J.M. (2009) Naturally occurring animal models with outer retina phenotypes. *Vision Res.*, **49**, 2636–2652.
12. Jeon, C.J., Strettoi, E. and Masland, R.H. (1998) The major cell populations of the mouse retina. *J. Neurosci.*, **18**, 8936–8946.
13. Koenekoop, R.K., Lopez, I., den Hollander, A.I., Allikmets, R. and Cremers, F.P. (2007) Genetic testing for retinal dystrophies and dysfunctions: benefits, dilemmas and solutions. *Clin. Exp. Ophthalmol.*, **35**, 473–485.
14. den Hollander, A.I., Roepman, R., Koenekoop, R.K. and Cremers, F.P. (2008) Leber congenital amaurosis: genes, proteins and disease mechanisms. *Prog. Retin. Eye Res.*, **27**, 391–419.
15. Hart, A.W., McKie, L., Morgan, J.E., Gautier, P., West, K., Jackson, I.J. and Cross, S.H. (2005) Genotype-phenotype correlation of mouse pde6b mutations. *Invest. Ophthalmol. Vis. Sci.*, **46**, 3443–3450.
16. McLaughlin, M.E., Sandberg, M.A., Berson, E.L. and Dryja, T.P. (1993) Recessive mutations in the gene encoding the beta-subunit of rod phosphodiesterase in patients with retinitis pigmentosa. *Nat. Genet.*, **4**, 130–134.
17. Schnütgen, F., De-Zolt, S., Van Sloun, P., Hollatz, M., Floss, T., Hansen, J., Altschmied, J., Seisenberger, C., Ghyselinck, N.B., Ruiz, P. *et al.* (2005) Genomewide production of multipurpose alleles for the functional analysis of the mouse genome. *Proc. Natl Acad. Sci. USA*, **102**, 7221–7226.
18. Horn, C., Hansen, J., Schnütgen, F., Seisenberger, C., Floss, T., Irgang, M., De-Zolt, S., Wurst, W., von Melchner, H. and Noppinger, P.R. (2007) Splinkerette PCR for more efficient characterization of gene trap events. *Nat. Genet.*, **39**, 933–934.
19. Codega, P., Della Santina, L., Gargini, C., Bedolla, D.E., Subkhankulova, T., Livesey, F.J., Cervetto, L. and Torre, V. (2009) Prolonged illumination up-regulates arrestin and two guanylate cyclase activating proteins: a novel mechanism for light adaptation. *J. Physiol.*, **587**, 2457–2472.
20. Zhang, H., Fan, J., Li, S., Karan, S., Rohrer, B., Palczewski, K., Frederick, J.M., Crouch, R.K. and Baehr, W. (2008) Trafficking of membrane-associated proteins to cone photoreceptor outer segments requires the chromophore 11-cis-retinal. *J. Neurosci.*, **9**, 4008–4014.
21. Livak, K.J. and Schmittgen, T.D. (2001) Analysis of relative gene expression data using real-time quantitative PCR and the 2(-Delta Delta C(T)) Method. *Methods*, **25**, 402–408.
22. Markwell, M.A., Haas, S.M., Bieber, L.L. and Tolbert, N.E. (1978) A modification of the Lowry procedure to simplify protein determination in membrane and lipoprotein samples. *Anal. Biochem.*, **87**, 206–210.
23. Miterski, B., Kruger, R., Wintermeyer, P. and Epplen, J.T. (2000) PCR/SSCP detects reliably and efficiently DNA sequence variations in large scale screening projects. *Comb. Chem. High Throughput Screen*, **3**, 211–218.
24. Petrasch-Parwez, E., Habbes, H.W., Weickert, S., Löbbecke-Schumacher, M., Wieczorek, S., Dermietzel, R. and Epplen, J.T. (2004) Fine-structural analysis and connexin expression in a transgenic model of Huntingtoń disease. *J. Comp. Neurol.*, **479**, 181–197.
25. Petrasch-Parwez, E., Nguyen, H.P., Löbbecke-Schumacher, M., Habbes, H.W., Wieczorek, S., Riess, O., Andres, K.H., Dermietzel, R. and von Hörsten, S. (2007) Cellular and subcellular localization of Huntington aggregates in the brain of a rat transgenic for Huntington disease. *J. Comp. Neurol.*, **501**, 716–730.
26. Lewald, J., Petrasch-Parwez, E.W. and Veh, R.W. (1994) GABA-like and Glutamate-like immunoreactivity in the pretecto-olivary pathway in the rat. *J. Hirnforsch.*, **35**, 279–294.
27. Harazny, J., Scholz, M., Buder, T., Lausen, B. and Kremers, J. (2009) Electrophysiological deficits in the retina of the DBA/2J mouse. *Doc. Ophthalmol.*, **119**, 181–197.
28. Peachey, N.S., Goto, Y., al-Ubaidi, M.R. and Naash, M.I. (1993) Properties of the mouse cone-mediated electroretinogram during light adaptation. *Neurosci. Lett.*, **162**, 9–11.